HHS Public Access

Author manuscript

J Am Soc Mass Spectrom. Author manuscript; available in PMC 2019 February 01.

Published in final edited form as:

J Am Soc Mass Spectrom. 2018 February ; 29(2): 230–241. doi:10.1007/s13361-017-1798-5.

Ion mobility spectrometry-mass spectrometry coupled with gas-phase hydrogen/deuterium exchange for metabolomics analyses

Hossein Maleki, **Ahmad K. Karanji**, **Sandra Majuta**, **Megan M. Maurer**, and **Stephen J. Valentine***

C. Eugene Bennett Department of Chemistry, West Virginia University, Morgantown, WV 26506, USA

Abstract

Ion mobility spectrometry - mass spectrometry (IMS-MS) in combination with gas-phase hydrogen/deuterium exchange (HDX) and collision-induced dissociation (CID) is evaluated as an analytical method for small-molecule standard and mixture characterization. Experiments show that compound ions exhibit unique HDX reactivities that can be used to distinguish different species. Additionally, it is shown that gas-phase HDX kinetics can be exploited to provide even further distinguishing capabilities by using different partial pressures of reagent gas. The relative HDX reactivity of a wide variety of molecules is discussed in light of the various molecular structures. Additionally, hydrogen accessibility scoring (HAS) and HDX kinetics modeling of candidate (*in-silico*) ion structures is utilized to estimate the relative ion conformer populations giving rise to specific HDX behavior. These data interpretation methods are discussed with a focus on developing predictive tools for HDX behavior. Finally, an example is provided in which ion mobility information is supplemented with HDX reactivity data to aid identification efforts of compounds in a metabolite extract.

Graphical Abstract

Correspondence to: Stephen Valentine; stephen.valentine@mail.wvu.edu.

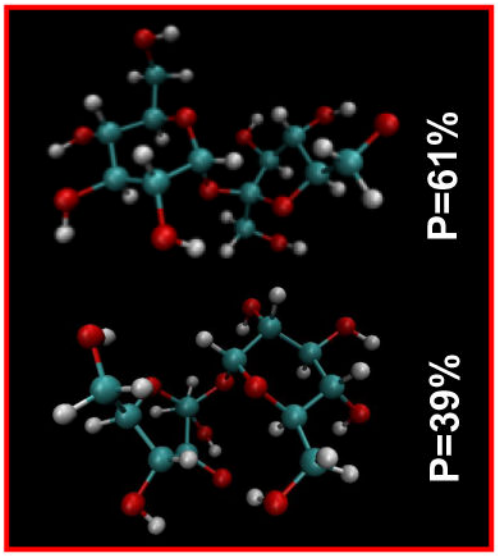

Introduction

Comparative metabolomics experiments can provide researchers with vital information regarding disease processes.[1–6] A goal of metabolomics investigations is the identification of new biomarkers for early disease diagnosis and the monitoring of disease progression. Biomarker discovery is accomplished through the comparison of identified metabolite abundances within biological samples (e.g., biofluids and tissues). As an example of the power of comparative metabolomics, consider that different types of coronary artery disease (CAD) can be differentiated by unique molecular profiles.[2] Understanding the bio-pathways implicated by changes in molecular concentrations as a function of physiological state may play a crucial role for developing effective treatments. Therefore, one suggested consequence of the effective metabolomics studies noted above would be the tailoring of therapeutic strategies for CAD.[2]

Characterization of metabolomics mixtures presents a number of challenges for analytical chemists resulting from the physicochemical diversity of metabolites (vis-à-vis functional groups, molecular structure, and molecular mass),[7–9] the existence of numerous isomers and isobars,[8] and the wide range in concentration of endogenous metabolites[10, 11]. Related to the latter characteristic, molecular concentration ranges in biofluids representing specific physiological states can span more than an order of magnitude.[10, 11] Together these properties present obstacles to high-throughput comparative metabolomics studies and invite the development of new technologies and techniques for complex mixture studies.

Ion mobility spectrometry (IMS) is a gas-phase separation technique in which ions traveling in a pressurized drift tube under the influence of a constant electric field are separated based on their shape and size.[27, 28] IMS-MS offers advantages in sensitivity by removing signals from low-intensity ions from the interfering signals of higher intensity species thereby increasing the overall measurement peak capacity.[29] This technique also enables the

separation of isomeric and isobaric species realizing some of the advantages of condensed-phase separations.[30–34] It has been proposed that the addition of collision cross section (CCS) data to metabolomics databases increases the identification accuracy.[43] Furthermore, two-dimensional (2D) plots of m/z vs t_D have shown that different classes of compounds can be relegated to distinct regions of analytical measurement space.[44] For example, classes of lipids can be easily distinguished from each other based on their occupation of such regions. Thus, IMS-MS has become an increasingly popular combination for studying metabolite mixtures.[35–424546] That said, IMS-MS analysis has two significant limitations for mixture characterization. IMS is a post-ionization separation step and thus still suffers from effects associated with competitive ionization. Additionally, ion mobilities are strongly correlated with m/z values limiting the overall separation capacity of the IMS-MS combination.

More than two decades ago, gas-phase hydrogen/deuterium exchange (HDX) coupled with MS (HDX-MS) was introduced as a structural analysis tool for protein and peptide ions.[47–49] This work was extended to include the study a wide array of different molecules.[50–56] The approach was also combined with IMS to provide shape and reactivity information for conformers of biological ions.[57, 58] More recently, with the development of non-ergodic ion fragmentation techniques, IMS-HDX-MS was used to determine relative deuterium uptake in a site-specific manner for peptide ions.[59, 60] From such studies, a question that has arisen is whether or not HDX profiles can be availed to aid in the characterization of complex mixtures of small molecules.

In a recent article, the usage of gas-phase HDX in combination with ion mobility techniques was proposed as a means for compound identification in ‘omics mixtures.[61] The work described various IMS-HDX measurements that could serve to provide unique identifiers for different molecular species and demonstrated the necessary robustness to be implemented in ‘omics workflows. In order to be useful as a predictive tool, the physicochemical properties of small molecules affecting HDX must be clearly elucidated. This work presents initial efforts to map such properties. Additionally, an example of how the approach would be used to aid identification of compounds in ‘omics mixtures is presented. Through these proof-of-principle studies, the utility of IMS-HDX-MS for metabolite identification is further explored.

EXPERIMENTAL SECTION

Sample preparation

Hydroxyproline, adenine, leucine, isoleucine homocysteine, glutamine, lysine, dopamine, sucrose and acetaminophen were purchased from Sigma Aldrich (St. Louis, MO) and used without further purification. The Avanti lipid mixture and the bovine heart extract were purchased from Avanti Polar Lipids Inc. (Alabaster, AL). Methanol, acetonitrile (ACN), methylene chloride, ammonium acetate and glacial acetic acid (HCOOH) were also purchased from Sigma-Aldrich (St. Louis, MO). Tables S1 and S2 in the Supporting Information section show the molecular structures of the compounds used in this study.

A number of single standard and mixture sample solutions were prepared to assess the HDX reactivities of a wide range of sample types both with respect to size and composition. The

small-molecule mixture consisted of lysine, acetaminophen, and dopamine. The single-standard solutions contained one of the small molecules (< 200 g/mole) listed above with the exception of sucrose. For the mixture and the single standard solutions, the concentration of the analytes was 0.01 mg/mL in methanol:acetonitrile (1:1). Acetic acid (1%) was added to enhance compound ionization. For preparation of the sucrose standard solution, 10 mg of standard was dissolved in 10 mL of water:acetonitrile (50:50) solution. Ammonium hydroxide (1%) was added to aid compound ionization.

In the study of lipids, three lipid mixture solutions were analyzed as well as the bovine heart extract. A lipid working solution was first prepared by mixing 250 mL of methylene chloride, 250 mL of methanol, and 5 mL of ammonium acetate solution (1 M solution prepared by dissolving 1.54 grams of ammonium acetate in 20 mL of methanol). The first lipid standard mixture was prepared by transferring 400 μL of Avanti lipid mix solution to a 20 mL glass vial and adding 3.6 mL of lipid working solution. The second lipid standard mixture contained the isobars 15:0 Lyso PC and 07:0 PC (DHPC). For this sample, 0.1 mg/mL of each standard solution was prepared by dissolving 1 mg of each standard into 10 mL of lipid working solution. The isobaric lipid mixture was prepared by adding 1 mL of each lipid standard solution. The third lipid mixture solution was prepared in identical fashion and contained the isomers (Δ9-Trans) PC (14:1/14:1) and (Δ9-Cis) PC (14:1/14:1). The bovine heart extract solution was prepared by using 400 μL of bovine heart extract and adding 3.6 mL of lipid working solution.

Instrumentation

For mobility measurements, an instrument consisting of a home-built drift tube coupled to a linear ion trap (LTQ Velos) mass spectrometer was used. The instrumentation has been described in detail elsewhere.[62] Briefly, samples were infused (400 nL/min) through a pulled-tip capillary which was biased at ±2000 V relative to the entrance of a desolvation region. The desolvation region houses an ion funnel trap[63, 64] where ions are stored and periodically (frequency of 50 Hz) released into the drift tube. Here ions separate under the influence of a constant electric field (10 V/cm). The drift tube contains He (300 K) at ~2.5 Torr. For HDX experiments, partial pressures of ~0.02 and ~0.04 Torr of D_2O were added to the He buffer gas via evaporation through a variable leak valve. The experiments for the metabolite standard, the lipid standard, and the bovine heart extract sample were performed in positive ESI mode. For the sucrose sample, experiments were performed in negative ion mode. CID experiments were performed by isolating a precursor ion with a *m/z* isolation window of ±1.0 Da relative to the centroid *m/z* value. Selected ions were fragmented using a normalized activation energy of 35.

Drift time (t_D)-resolved mass spectra were created with the application of a gating pulse to a Tyndall gate at the back of the drift tube. This gating pulse was delayed with respect to the ion introduction pulse setting the t_D of each mass spectrum. The delay was scanned across the entire t_D range using a step size of 0.1 ms. Each mass spectrum was converted to a text file and in-house software was used to assemble a 3-column array file containing t_D, *m/z*, and intensity (*i*) values. The DPlot software suite (HydeSoft Computing, Vicksburg, Mississippi) was used for the generation of 2D plots of *m/z* and t_D values. Using 2D t_D, *m/z*

plots as a guide, in house software was used to extract t_D-resolved isotopic distributions for individual dataset features.

Experimental collision cross sections (Ω) were calculated using the following expression:[65]

$$\Omega = \frac{(18\pi)^{1/2}}{16}\frac{ze}{k_B T^{1/2}}\left[\frac{1}{m_i}+\frac{1}{m_b}\right]^{\frac{t_D E}{L}}\frac{760}{P}\frac{T}{273.2}\frac{1}{N}, \quad 1)$$

where ze is the charge of the ion, E is the electric field strength, T is the temperature of the buffer gas, k_b is Boltzmann's constant, and m_i and m_b are the masses of the ion and the buffer gas, respectively. L is the length of the drift tube, P is the pressure of the buffer gas, and N is the number density of the buffer gas at STP. All experimental measurements were recorded using a constant-field drift tube (DT) while employing helium (He) as a buffer gas. Therefore, using the standard nomenclature, cross section values (experimental and theoretical) are referred to as $^{DT}CCS_{He}$.

Simulated annealing and HDX kinetics modeling

Sucrose ions having two different deprotonation sites were generated using the Avogadro software suite. Sites of deprotonation were -OH3 and -OH6 moieties (on the fructose monomer) as shown in Figure S1. Both ions were subjected to simulated annealing using the NAMD software suite. To accomplish this, the ions were heated instantaneously to 1000 K, maintained at 1000 K for 40 ps, and cooled to 50 K over 40 ps. The 50 K structures were then energy-minimized and the resulting structure was saved for CCS calculation. This same structure served as the starting point for the next round of simulated annealing. This was performed for 1000 cycles to generate 1000 candidate structures. $^{DT}CCS_{He}$ values were computed for all structures using the trajectory method in the MOBCAL software.[66, 67] One structure from each charge site configuration having a $^{DT}CCS_{He}$ value near that observed experimentally was selected for HDX kinetics modeling.

HDX kinetics were modeled using a modified hydrogen accessibility scoring (HAS) approach.[68] Briefly, the contribution of each heteroatom site to the ion's measured HDX rate was scaled according to two factors. The first factor was the distance of the site to the charge site in which values scaled according to inverse distance. Using these values, all heteroatom sites were then normalized to provide fractional contribution to the overall HDX rate. Next, because distance alone does not describe accessibility, a second factor was used to scale each of the HDX rate contribution scores. This factor was considered based on whether or not the charge site could access the exchange site via molecular motion as well as whether or not the exchange site was involved in significant intramolecular hydrogen bonding. After scaling the individual contributions to HDX rate, the HDX process was modeled for each conformer using an approach described previously.[68] The theoretical isotopic distributions were then calculated for the two different ion conformer types.

The best-fit isotopic distribution obtained from contributions by both conformer types was computed using a pseudo Monte Carlo approach. Here, random, fractional contributions

from both theoretical isotopic distributions were evaluated in an iterative manner. The fit did not improve after 1×10^5 iterations. The in house software then provided the contribution by each conformer type to the best-fit isotopic distribution.

RESULTS AND DISCUSSION

Compound specific HDX behavior

To best provide unique compound identifiers, an analytical technique must yield a measurement that is orthogonal to each of the other separate measurements. That is, the new measurement must not exhibit significant correlation to other measurements. To demonstrate such a feature for HDX with respect to ion mobility measurements consider the deuterium uptake of $[M+H]^+$ acetaminophen, dopamine, and lysine ions as shown in Figure 1. These ions were selected to demonstrate variable reactivities for species of relatively similar molecular weight. Additionally, because isotopic distributions tend to broaden upon HDX, acetaminophen and dopamine being of more similar molecular weight offer a test case for resolution of ion signatures. $^{DT}CCS_{He}$ values for these ions are provided in Table 1. Upon introduction of ~0.02 Torr of D_2O into the drift tube, the major isotopologue peaks demonstrate an incorporation of 6, 1, and 0 deuteriums for lysine, acetaminophen, and dopamine, respectively.

Considering the limited number of heteroatom hydrogens for many small-molecule metabolites, a question of utility arises. That is, if many compounds of similar mass have only 2 exchangeable hydrogens, how can such an approach be useful? To show utility requires a brief discussion of HDX kinetics. The mechanism of HDX requires the formation of a long-lived reaction intermediate involving the charge site and a less basic site on the molecule.[58, 69] Therefore, in addition to atomic composition, the ion structure (in terms of the relative positions of charge and exchange sites) dictates the rate of HDX of the ions and thus the amount of incorporated deuterium. It might be expected then that the rates of exchange are nearly as diverse as the compound types encountered in the mixture. Indeed such variability in HDX behavior is demonstrated in Figure 1. For these ions as well as others examined in this study, different structural attributes result in unique isotopic distributions with characteristic intensities for the M+0, M+1, M+2, etc. isotopologue peaks.

Because of differences in rates of exchange, the ions may also exhibit unique HDX behavior at different partial pressure settings of D_2O. Figure S2 shows the HDX behavior of mobility-selected ions at D_2O partial pressures of ~0.02 and ~0.04 Torr. Upon addition of ~0.02 Torr D_2O, mobility-selected $[M+H]^+$ hydroxyproline ions exhibit an isotopic distribution in which the M+1 peak is the dominant feature and the M+0 peak is largely absent (Figure S2A). With the same partial pressure of D_2O, $[M+H]^+$ 18:1 Lyso PC ions produce an isotopic distribution in which the M+0 peak is yet the dominant feature with a nearly equivalent amount of the M+1 peak (Figure S2C). The M+3 peak is ~30% of the height of the M+1 peak. Upon increasing the D_2O partial pressure to ~0.04 Torr, the isotopic features for the singly-charged hydroxyproline do not change in relative intensity (Figure S2B). At this same partial pressure setting, the singly-charged ions of 18:1 Lyso PC produce an isotopic distribution in which the most intense feature is the M+2 peak and the M+3 peak is also a major (~30%) constituent (Figure S2D).

Other ions show isotopic distributions that are more similar at the two different partial pressure settings. For example, $[M+H]^+$ 14:1 PE and M^+ 18:1 SM ions show similar isotopic patterns upon introduction of 0.02 Torr of D_2O. For each, the major peak is the M+0 peak; however, for both ion types, there is a noticeable –but similar –increase in the M+1 peak (Figures S2E and S2G). After increasing the partial pressure of D_2O to ~0.04 Torr, both ion types show isotopic distributions in which the M+1, M+2, and M+3 peaks are major constituents. Uniquely for the 14:1 PE ions, the M+4 peak is the dominant feature. Such a bimodal distribution could be indicative of the HDX behavior of different conformer types.[49] Indeed, in the He buffer gas, two conformers are resolved (Figure S3 in the Supporting Information section). However, these conformers are not resolved in the He:D_2O mixture. That said, even for slowly-exchanging conformer types, the 14:1 PE and the 18:1 SM ions show some difference. For example the M+3 peak shows a greater relative intensity for the former ions compared to the latter ions upon increasing the partial pressure of D_2O.

Distinguishing isobaric ions

Considering the implementation of IMS-HDX with a low-resolution mass spectrometer, it is necessary that isobaric ions exhibit differences in HDX uptake. To provide examples of differences in HDX behavior for isobaric ions, data have been recorded for $[M+H]^+$ adenine, homocysteine, lysine, and glutamine ions as shown in Figure 2. The adenine and homocysteine ions have the same nominal m/z value of 136. Upon addition of D_2O (~0.04 Torr) to the drift tube, a portion of the adenine ions undergo HDX producing a bimodal distribution in which the dominant peaks in the isotopic distribution become the M+0 and M +2 peaks (Figure 2A). In contrast, for homocysteine ions the dominant peak in the isotopic distribution becomes the M+1 peak (Figure 2B). As mentioned above, lysine ions undergo significant HDX with the M+6 peak being the dominant feature in the isotopic distribution (Figure 2C). In contrast, for glutamine ions the dominant peak in the isotopic distribution becomes the M+1 peak (Figure 2D).

Figures 1 and 2 present results for which the major isotopic peaks at specific t_D values could be used to distinguish different ions. Higher molecular weight species can present a greater challenge especially as the isotopic distribution becomes broader. Figure 3 shows mobility-selected isotopic distributions obtained upon HDX experiments for a two-component lipid mixture. The mixture contains the lipid isobars 15:0 Lyso PC and 07:0 PC (DHPC) having a nominal m/z of 482. From the compound structures in Table S2 it is evident that the maximum number of exchangeable hydrogens for the respective lipid ions are 2 and 1. For comparison, the isotopic distributions obtained from HDX experiments of the separate isobaric lipids are shown in Figure S4. The respective lipid ions yield $^{DT}CCS_{He}$ values of 155.3 $Å^2$ and 156.9 $Å^2$ (Table 1) and are not resolved in the mobility measurement in which He or He and D_2O buffer gas is used. However, for HDX experiments, clear differences in isotopic distributions are observed at select drift times. As shown in Figure 3, the M+1 isotopologue peak is the major feature observed at a drift time selection of 10.8–11.0 ms. At 11.2–11.4 ms, the M+2 isotopologue peak is of nearly equal abundance while at 11-4–11.6 ms it becomes the dominant feature in the distribution. This change in the distribution is consistent with a mobility selection that is dominated by 07:0 PC (DHPC) ions at shorter t_D values and then becomes dominated by the 15:0 Lyso PC at longer times. Admittedly, the

HDX approach may be of limited value for isomeric lipid ions (as well as small-molecule isomers) having the same cross section. The $[M+H]^+$ (Δ9-Trans) PC (14:1/14:1) and (Δ9-Cis) PC (14:1/14:1) ions show similar deuterium uptake values as is also observed for leucine and isoleucine ions (Figures S5 and S6). For the lipids, this is somewhat expected as the head group is identical for this species and the ions under HDX for the same amount of time.

HDX behavior of lipid ions

The M^+ and $[M+H]^+$ lipid ions (Table S2) also display unique HDX behavior as shown in Figure 4. In summary, ions produce isotopic distributions in which M+1, M+2, or M+3 peaks are the dominant species. For example, the 18:1 Lyso PC ions produce an isotopic distribution in which the M+2 peak is the dominant peak upon introduction of ~0.04 Torr of D_2O (Figure 4A). The M+3 peak is also present with a relative intensity of ~30%. In comparison, the 18:1 Ceramide ions yield a broader isotopic distribution where the M+3 peak is the dominant feature (Figure 4B). M+1, M+2, and M+4 peaks also comprise the distribution having relative intensities of 16%, 45%, and 35%, respectively.

With the addition of ~0.04 Torr D_2O, the 14:1 PE, PC (14:1/14:1), and 18:1 SM ions all display isotopic distributions having dominant M+1 peaks. As mentioned above, the 14:1 PE ions also produce a large M+4 peak and the bimodal distribution may result from two different ion conformer types that are mobility resolved in He buffer gas (Figure S3). For the purposes of comparison to the other lipids, the discussion here is focused on the lower *m*/z features. A comparison of the isotopic distributions of these ions shows differences in the relative intensities of the M+2 and M+3 peaks. For the former ions, the relative intensities are 58% (Figure 4C), 42% (Figure 4D), and 70% (Figure 4E) for the 14:1 PE, PC (14:1/14:1), and 18:1 SM ions, respectively. For the M+3 peaks the respective intensities are 37%, 9%, and 22%. A question that arises is whether or not such differences are significant; that is, can such differences be used to obtain reliable identifications? Extensive experiments have shown that such disparity in isotopic distributions is significant as run-to-run comparisons yield root mean square displacement values of <1.5%.[61] Finally, it is noted that no deuterium uptake is observed for the sodiated form of the lipids as shown in Figure S7 in the Supporting Information section. This can be explained by the fact that the sodium cannot participate in the hydrogen-bonded intermediate of the relay mechanism.[70]

Structural explanations for HDX behavior

Significant effort has been exerted to develop collision cross section databases for small molecules.[46, 71–74] It has been proposed that such databases could find utility in ion identification either through direct matching of ion mobilities or through the locating of an ion's mobility to an analytical region that is associated with a family of compounds.[44, 75] Previously, it was proposed that the matching of isotopic distributions upon HDX could be used in this fashion where comparisons would be made to database compounds.[61] One potential advantage of ion mobility techniques is that, to some degree, measurement predictions are accessible for unknown compounds. Such approaches range from the consideration of substituent contributions to mobility to the use of powerful quantum mechanics and molecular dynamics approaches to obtain structures for cross section

calculation comparison.[76–78] Adding to the capability of HDX prediction to an IMS prediction method could provide a powerful tool for the identification of unknown compounds.

In order to develop predictive tools for HDX behavior, it is important to elucidate the factors governing the reaction process. Because the HDX mechanism requires the formation of a long-lived reaction intermediate involving the charge site and a less basic [58, 69], it is important to first consider site that are both accessible to collisions with D_2O elements of compound structure that favor or disfavor intermediate formation to explain ion reaction behavior. As described above, $[M+H]^+$ dopamine ions do not undergo HDX even at the highest partial pressure settings of D_2O (Figure 1B). This is observed despite the fact that such ions have 5 heteroatom hydrogens. From the molecular structure (Table S1), it can be argued that exchange does not occur because D_2O cannot hydrogen bond at the charge site and a less basic hydroxyl as these substituents are located distantly (from the charge site) across the aromatic ring. Thus, the relay mechanism is not in effect and HDX is not achieved. In contrast, the flexibility of the side chain of the lysine ions permits the positioning of the charge in relative proximity of a less basic site (e.g., carbonyl) such that HDX proceeds efficiently (Figure 1B). The incorporation of 1 deuterium for the $[M+H]^+$ acetaminophen ions would then require increased access of the less basic site to the charge site despite being located across the aromatic ring. In this case the charge site is closer to the less basic site compared with the dopamine ions.

For singly-charged adenine ions, there are 4 heteroatom hydrogens. Upon addition of ~0.04 Torr of D_2O, a bimodal distribution is produced where one dominant feature in the isotopic distribution is the M+0 peak and the other is the M+2 peak (Figure 2A). It is possible that the bimodal distribution results from two different charge arrangements - one in which the charge resides on the primary amine and the other in which it resides on the aromatic ring shown in Table S1. The lack of exchange of all 4 hydrogens in both isotopic distributions can be ascribed to the fact that the heteroatom hydrogens are relatively distant to one another. Singly-charged glutamine ions have 6 heteroatom hydrogens. These ions exhibit a relatively small degree of HDX as shown in Figure 2D. Because the heteroatom hydrogens reside at the end of the side chain and the N- and C-termini, the data suggest that these ions are less flexible in that the charge site does not approach the other heteroatom sites as efficiently as is observed for lysine. Providing a rationale for HDX behavior of homocysteine ions based on compound structure (Table S1) is more challenging. These ions have 5 heteroatom hydrogens and the dominant feature in the isotopic distribution is the M +1 peak. Considering that the charge would reside at the amino terminus and thus present significant redundancy in exchangeable hydrogens, the low level of exchange suggests accessibility to the side chain or C-terminal hydrogen alone.

For the lipids (Figure 4), the 18:1 Lyso PC ions have 2 heteroatom sites. The isotopic distribution shows nearly complete exchange with the M+2 peak being the dominant feature. This can be reasoned by the fact that both sites are near less basic sites onto which the deuterium can be shuttled via the relay mechanism. The 18:1 Ceramide ions have 4 heteroatom hydrogens and the dominant feature in the isotopic distribution is the M+3 peak. Additionally, the presence of significant M+1 and M+2 peaks indicates lower HDX

efficiency. Assuming that the charge resides at the secondary amine, the HDX behavior can be explained by less accessibility of the terminal hydroxyl group to the less basic carbonyl site for example. Here the carbonyl site would serve as the less basic site onto which the deuterium is originally shuttled via the relay mechanism. For the 14:1 PE ions, there are 4 heteroatom hydrogens. The isotopic distribution is bimodal with dominant features corresponding to the M+1 and M+4 peaks. The latter must arise from an ion conformer type in which the protonated primary amine has access to a less basic site allowing transfer of the incorporated deuterium back to the charge site. The conformer type leading to the M+1 peak being the dominant feature must necessarily allow less access of the terminal amine to a less basic site. Again it is noted that two conformer types are resolved by IMS alone. (Figure S3) The 14:1 PC ions have only 1 heteroatom hydrogen which exchanges efficiently; the M+1 peak is the dominant feature. This is similar to the high-efficiency exchange of the phosphate hydrogen for the 18:1 Lyso PC ions suggesting facile formation of the reaction intermediate at the site of the phosphate group. Finally, the 18:1 SM ions have 4 heteroatom hydrogens. Overall, the HDX efficiency of some sites is low as the isotopic distribution is dominated by the M+1 peak with the M+2 peak contributing to the distribution as well. In this case it is possible that the secondary amine – which is not protonated for these ions – and the hydroxyl group are less accessible to either the formation of the reaction intermediate or to the less basic site serving as the original site of deuterium incorporation.

The HDX behavior of the ions shown in Figures 1–4 has been described in terms of the ability of different heteroatom sites to participate in the reaction intermediate involved in the relay mechanism or their relative accessibility to the original site of deuterium incorporation. Thus a cursory examination of the molecular structure represents the beginning of the development of HDX prediction capability for compounds for which measurements have not been obtained. That said, although a cursory examination of compound structure may help to describe the observed reactivity, for certain ions, this may be more difficult. For example, bimodal distributions coupled with considerations of exchange site redundancy is used above to suggest the presence of different conformer types (including charge site configuration). For some species a clear distinction in multiple conformer types may not be drawn easily from the isotopic distribution or the mobility distribution. For example, the differences in *m/z* range of the isotopic distributions could suggest that some ion populations are comprised of greater structural heterogeneity (conformer types).[68] That is, as with the bimodal distributions discussed above, it is possible that different conformer types could give rise to the broad isotopic distribution observed for the 18:1 Ceramide ions (Figure 4).

To consider the effect of multiple, unresolved conformers, $[M\text{-}H]^-$ sucrose ions have been studied. Even though these ions exhibit a single conformer type in the mobility distribution (Table 1), a broad isotopic distribution is observed in which the dominant peaks are the M +0, M+1, M+2, M+3, and M+4 species as illustrated in Figure 5. The presence of lower *m/z* peaks suggests that at least one sucrose ion conformer type shows limited access to exchange sites. One explanation could be that different charge site configurations result in conformers that exhibit varying degrees of accessibility to exchange sites. Simulated annealing of deprotonated ions produces several conformers with collision cross sections that match that observed experimentally. Two conformer types with different charge sites were selected for HDX modeling (see Experimental section above). Conformer 1 (Figure

S1A), being deprotonated at the –OH3 site, is charge solvated by hydroxyl groups at the –OH1, –OH2, –OH4, and –OH5 moieties. Conformer 2 (Figure S1B), being deprotonated at the –OH6 site, is solvated by the –OH7 hydroxyl moiety. Other sites are not easily accessed by the charge site for this conformer as determined by modified HAS scoring (see Experimental section). Using the simulated isotopic distributions from the two conformers and a pseudo Monte Carlo best-fit approach, the optimal populations of the two candidate conformers have been computed. The best-fit isotopic distribution as shown in Figure 5 suggests that Conformer types 1 and 2 would contribute to the overall HDX behavior with a respective 0.63:1 ion population ratio. That said, the best-fit approach does not accurately capture the intensity of the M+4 peak. It is also possible that other conformer types of lower abundance are present allowing for increased HDX.

From the analysis above, the range of HDX behavior across metabolite space is expected to be as diverse as the differences in the types of compound substituents and their locations in ion structures. It is stressed that even though the same isotopologues may be the dominant features in the different HDX patterns, their relative intensities can be significantly different (e.g., Figure 4). It is this diversity that offers the opportunity for using HDX in conjunction with IMS and MS for compound identification. That said, the magnitude of the challenge in developing predictive HDX tools becomes readily apparent with this level of diversity as well. Herculean effort will be required to populate experimental databases and utilize high-quality *in-silico* structures to develop such tools.

Proof-of-principle application of HDX data for compound identification efforts

It is instructive to consider how the IMS-HDX approach might be used for ‘omics mixture characterization. Figure S8A shows the isotopic distribution after HDX of an unknown compound from the bovine heart extract sample. Here the dominant species are the M+1 ions. There are also significant contributions to the distribution from the M+0 and M+2 ions. This is very similar to the isotopic distribution obtained for the precursor ions of hydroxyproline. Additionally, the $^{DT}CCS_{He}$ value for the unknown ions is 58.6 which is near that determined for hydroxyproline (Table 1). Therefore, based on IMS-HDX-MS data alone, a match would be obtained for hydroxyproline. However, a comparison of the CID data for the unknown ions and hydroxyproline ions reveals a major difference as shown in Figure S8C and S8D, respectively. Notably, an intense ion at m/z 90 is present in the fragmentation spectrum for the unknown feature in the bovine sample. This ion is completely absent in the fragmentation spectrum of hydroxyproline. Notably, parallel CID[79] with HDX and deuterium scrambling with HDX have been presented previously as a means to provide other unique identifiers.[61] These methods can also be implemented without adding significant experimental time to create an IMS-HDX-MS/MS approach. In that manner, high-throughput analyses could be availed to eliminate false positive assignments. It is also noted that the post-HDX isotopic patterns of leucine and isoleucine (m/z 132.2) as shown in Figure S5 do not match that (Figure S8) of the unknown compound providing another example of how this approach aids identification efforts.

In a separate example, a dataset feature (m/z 147.2) from the bovine heart extract is observed to have a $^{DT}CCS_{He}$ value of 64.3 A^2. Upon adding ~0.04 Torr of D_2O, the ion produces an

isotopic distribution in which the M+6 peak is the dominant feature (Figure 6A). Indeed the distribution is very similar to that observed for lysine ions (Figure 6B). Additionally, the $^{DT}CCS_{He}$ value matches that determined for singly-charged lysine ions (Table 1). To support such an assignment, the precursor ions from the bovine heart extract have been isolated and subjected to CID. The dominant fragments are produced by the neutral loss of -NH_3 and -H_2O. Low-intensity fragment ions are observed at m/z 82 and 103. The same dominant and low-intensity fragment ions are produced upon CID of mobility-selected lysine ions. This analysis would support the assignment of the unknown ions as lysine ions in the heart extract sample. One advantage to the assignment of the ions based on the IMS-HDX-MS information alone is that such information can be obtained from dispersive measurements on very short timescales (seconds). That is, no ion selection or m/z or mobility scanning is required with currently available commercial instrumentation.

Conclusions

Proof-of-principle experiments have been conducted to demonstrate the utility of IMS combined with gas-phase HDX and MS analysis. The work demonstrates that, despite limited numbers of heteroatom hydrogens on many small molecules, unique isotopic distributions are produced. Such selectivity results from differences in HDX kinetics arising from the relative three-dimensional positions of the heteroatoms and charge sites within the various compounds. Although the wide range of different structural arrangements offers great opportunity with regard to selectivity, it presents significant challenges with regard to deciphering the rules governing HDX. Elucidating such rules is necessary to develop accurate tools for predicting HDX behavior. The value of the ability to accurately predict HDX behavior cannot be overstated. Such an approach can be combined with IMS prediction methods [77, 80] to suggest assignments of heretofore unmeasured compounds. These could include species such as newly emerging neuropeptides or drugs of abuse. Therefore, the careful study of the HDX behavior of numerous database compounds should be a significant pursuit in the future.

Supplementary Material

Refer to Web version on PubMed Central for supplementary material.

Acknowledgments

We are grateful for financial support from the National Science Foundation (CHE-1553021).

References

1. Ko WH, Tsou YJ, Lin MJ, Chern LL. Activity and characterization of secondary metabolites produced by a new microorganism for control of plant diseases. New Biotechnology. 2010; 27(4): 397–402. [PubMed: 20580869]
2. Fan Y, Li Y, Chen Y, Zhao YJ, Liu LW, Li J, Wang SL, Alolga RN, Yin Y, Wang XM, Zhao DS, Shen JH, Meng FQ, Zhou X, Xu H, He GP, Lai MD, Li P, Zhu W, Qi LW. Comprehensive Metabolomic Characterization of Coronary Artery Diseases. Journal of the American College of Cardiology. 2016; 68(12):1281–1293. [PubMed: 27634119]

3. Alonso A, Julia A, Vinaixa M, Domenech E, Fernandez-Nebro A, Canete JD, Ferrandiz C, Tornero J, Gisbert JP, Nos P, Casbas AG, Puig L, Gonzalez-Alvaro I, Pinto-Tasende JA, Blanco R, Rodriguez MA, Beltran A, Correig X, Marsal S. Consortium I. Urine metabolome profiling of immune-mediated inflammatory diseases. Bmc Medicine. 2016:14. [PubMed: 26822124]
4. Oresic M, Vidal-Puig A, Hanninen V. Metabolomic approaches to phenotype characterization and applications to complex diseases. Expert Review of Molecular Diagnostics. 2006; 6(4):575–585. [PubMed: 16824031]
5. Jarmusch AK, Pirro V, Baird Z, Hattab EM, Cohen-Gadol AA, Cooks RG. Lipid and metabolite profiles of human brain tumors by desorption electrospray ionization-MS. Proceedings of the National Academy of Sciences of the United States of America. 2016; 113(6):1486–1491. [PubMed: 26787885]
6. Vizcaino MI, Engel P, Trautman E, Crawford JM. Comparative Metabolomics and Structural Characterizations Illuminate Colibactin Pathway-Dependent Small Molecules. Journal of the American Chemical Society. 2014; 136(26):9244–9247. [PubMed: 24932672]
7. Kotera M, McDonald AG, Boyce S, Tipton KF. Functional Group and Substructure Searching as a Tool in Metabolomics. Plos One. 2008; 3(2)
8. Dettmer K, Aronov PA, Hammock BD. Mass spectrometry-based metabolomics. Mass Spectrometry Reviews. 2007; 26(1):51–78. [PubMed: 16921475]
9. Mirnaghi FS, Caudy AA. Challenges of analyzing different classes of metabolites by a single analytical method. Bioanalysis. 2014; 6(24):3393–3416. [PubMed: 25534794]
10. Wishart DS, Tzur D, Knox C, Eisner R, Guo AC, Young N, Cheng D, Jewell K, Arndt D, Sawhney S, Fung C, Nikolai L, Lewis M, Coutouly MA, Forsythe I, Tang P, Shrivastava S, Jeroncic K, Stothard P, Amegbey G, Block D, Hau DD, Wagner J, Miniaci J, Clements M, Gebremedhin M, Guo N, Zhang Y, Duggan GE, MacInnis GD, Weljie AM, Dowlatabadi R, Bamforth F, Clive D, Greiner R, Li L, Marrie T, Sykes BD, Vogel HJ, Querengesser L. HMDB: the human metabolome database. Nucleic Acids Research. 2007; 35:D521–D526. [PubMed: 17202168]
11. Wishart DS, Jewison T, Guo AC, Wilson M, Knox C, Liu YF, Djoumbou Y, Mandal R, Aziat F, Dong E, Bouatra S, Sinelnikov I, Arndt D, Xia JG, Liu P, Yallou F, Bjorndahl T, Perez-Pineiro R, Eisner R, Allen F, Neveu V, Greiner R, Scalbert A. HMDB 3.0-The Human Metabolome Database in 2013. Nucleic Acids Research. 2013; 41(D1):D801–D807. [PubMed: 23161693]
12. Alonso R, Marsal S, Julia a. Analytical Methods in Untargeted Metabolomics: State of the Art in 2015. 2015; 3:23.
13. Griffiths WJ, Koal T, Wang YQ, Kohl M, Enot DP, Deigner HP. Targeted Metabolomics for Biomarker Discovery. Angewandte Chemie-International Edition. 2010; 49(32):5426–5445. [PubMed: 20629054]
14. Guleria A, Pratap A, Dubey D, Rawat A, Chaurasia S, Sukesh E, Phatak S, Ajmani S, Kumar U, Khetrapal CL, Bacon P, Misra R, Kumar D. NMR based serum metabolomics reveals a distinctive signature in patients with Lupus Nephritis. Scientific Reports. 2016:6. [PubMed: 28442741]
15. Li BQ, Xu ML, Wang X, Zhai HL, Chen J, Liu JJ. An approach to the simultaneous quantitative analysis of metabolites in table wines by H-1 NMR self-constructed three-dimensional spectra. Food Chemistry. 2017; 216:52–59. [PubMed: 27596391]
16. Moutloatse GP, Bunders MJ, van Reenen M, Mason S, Kuijpers TW, Engelke UFH, Wevers RA, Reinecke CJ. Metabolic risks at birth of neonates exposed in utero to HIV-antiretroviral therapy relative to unexposed neonates: an NMR metabolomics study of cord blood. Metabolomics. 2016; 12(11)
17. Picone G, Savorani F, Trimigno A, Mezzetti B, Capozzi F, Engelsen SB. Metabolic changes of genetically engineered grapes (Vitis vinifera L.) studied by H-1-NMR, metabolite heatmaps and iPLS. Metabolomics. 2016; 12(10)
18. Ullrich SF, Averesch NJH, Castellanos L, Choi YH, Rothauer A, Kayser O. Discrimination of wild types and hybrids of Duboisia myoporoides and Duboisia leichhardtii at different growth stages using H-1 NMR-based metabolite profiling and tropane alkaloids-targeted HPLC-MS analysis. Phytochemistry. 2016; 131:44–56. [PubMed: 27567452]

19. Nicholson JK, Lindon JC, Holmes E. ‘Metabonomics’: understanding the metabolic responses of living systems to pathophysiological stimuli via multivariate statistical analysis of biological NMR spectroscopic data. Xenobiotica. 1999; 29(11):1181–1189. [PubMed: 10598751]
20. Johnson AR, Carlson EE. Collision-Induced Dissociation Mass Spectrometry: A Powerful Tool for Natural Product Structure Elucidation. Analytical Chemistry. 2015; 87(21):10668–10678. [PubMed: 26132379]
21. Ashline DJ, Yu Y, Lasanajak Y, Song XZ, Hu LY, Ramani S, Prasad V, Estes MK, Cummings RD, Smith DF, Reinhold VN. Structural Characterization by Multistage Mass Spectrometry (MSn) of Human Milk Glycans Recognized by Human Rotaviruses. Molecular & Cellular Proteomics. 2014; 13(11):2961–2974. [PubMed: 25048706]
22. Murphy RC, Axelsen PH. MASS SPECTROMETRIC ANALYSIS OF LONG-CHAIN LIPIDS. Mass Spectrometry Reviews. 2011; 30(4):579–599. [PubMed: 21656842]
23. Sumner LW. Current Status and Forward Looking Thoughts on LC/MS Metabolomics. Plant Metabolomics. 2006; 57:21–32.
24. t’Kindt R, Van Bocxlaer J. LC-MS BASED METABOLOMICS. 2009:39–73.
25. Kanani H, Chrysanthopoulos PK, Klapa MI. Standardizing GC-MS metabolomics. Journal of Chromatography B-Analytical Technologies in the Biomedical and Life Sciences. 2008; 871(2): 191–201.
26. Welthagen W, Shellie RA, Spranger J, Ristow M, Zimmermann R, Fiehn O. Comprehensive two-dimensional gas chromatography-time-of-flight mass spectrometry (GC x GC-TOF) for high resolution metabolomics: biomarker discovery on spleen tissue extracts of obese NZO compared to lean C57BL/6 mice. Metabolomics. 2005; 1(1):65–73.
27. Stlouis RH, Hill HH. ION MOBILITY SPECTROMETRY IN ANALYTICAL-CHEMISTRY. Critical Reviews in Analytical Chemistry. 1990; 21(5):321–355.
28. Mason, EA., McDaniel, EW. Transport properties of ions in gases. 99. Wiley-VCH; New York: 1988.
29. Counterman AE, Hilderbrand AE, Barnes CAS, Clemmer DE. Formation of peptide aggregates during ESI: Size, charge, composition, and contributions to noise. Journal of the American Society for Mass Spectrometry. 2001; 12(9):1020–1035.
30. Valentine SJ, Counterman AE, Hoaglund CS, Reilly JP, Clemmer DE. Gas-phase separations of protease digests. Journal of the American Society for Mass Spectrometry. 1998; 9(11):1213–1216. [PubMed: 9794086]
31. McLean JA, Ruotolo BT, Gillig KJ, Russell DH. Ion mobility-mass spectrometry: a new paradigm for proteomics. International Journal of Mass Spectrometry. 2005; 240(3):301–315.
32. Ruotolo BT, Gillig KJ, Woods AS, Egan TF, Ugarov MV, Schultz JA, Russell DH. Analysis of phosphorylated peptides by ion mobility-mass spectrometry. Analytical Chemistry. 2004; 76(22): 6727–6733. [PubMed: 15538797]
33. Wu C, Siems WF, Klasmeier J, Hill HH. Separation of isomeric peptides using electrospray ionization/high-resolution ion mobility spectrometry. Analytical Chemistry. 2000; 72(2):391–395. [PubMed: 10658335]
34. Pu Y, Ridgeway ME, Glaskin RS, Park MA, Costello CE, Lin C. Separation and Identification of Isomeric Glycans by Selected Accumulation-Trapped Ion Mobility Spectrometry-Electron Activated Dissociation Tandem Mass Spectrometry. Analytical Chemistry. 2016; 88(7):3440–3443. [PubMed: 26959868]
35. Hines KM, May JC, McLean JA, Xu LB. Evaluation of Collision Cross Section Calibrants for Structural Analysis of Lipids by Traveling Wave Ion Mobility-Mass Spectrometry. Analytical Chemistry. 2016; 88(14):7329–7336. [PubMed: 27321977]
36. Kaplan K, Dwivedi P, Davidson S, Yang Q, Tso P, Siems W, Hill HH. Monitoring Dynamic Changes in Lymph Metabolome of Fasting and Fed Rats by Electrospray Ionization-Ion Mobility Mass Spectrometry (ESI-IMMS). Analytical Chemistry. 2009; 81(19):7944–7953. [PubMed: 19788315]
37. Kyle JE, Zhang X, Weitz KK, Monroe ME, Ibrahim YM, Moore RJ, Cha J, Sun XF, Lovelace ES, Wagoner J, Polyak SJ, Metz TO, Dey SK, Smith RD, Burnum-Johnson KE, Baker ES. Uncovering

biologically significant lipid isomers with liquid chromatography, ion mobility spectrometry and mass spectrometry. Analyst. 2016; 141(5):1649–1659. [PubMed: 26734689]

38. Vautz W, Nolte J, Fobbe R, Baumbach JI. Breath analysis-performance and potential of ion mobility spectrometry. Journal of Breath Research. 2009; 3(3)
39. Dwivedi P, Puzon G, Tam M, Langlais D, Jackson S, Kaplan K, Siems WF, Schultz AJ, Xun LY, Woodsd A, Hill HH. Metabolic profiling of Escherichia coli by ion mobility-mass spectrometry with MALDI ion source. Journal of Mass Spectrometry. 2010; 45(12):1383–1393. [PubMed: 20967735]
40. Knapman TW, Berryman JT, Campuzano I, Harris SA, Ashcroft AE. Considerations in experimental and theoretical collision cross-section measurements of small molecules using travelling wave ion mobility spectrometry-mass spectrometry. International Journal of Mass Spectrometry. 2010; 298(1–3):17–23.
41. Pang XQ, Jia CX, Chen ZW, Li LJ. Structural Characterization of Monomers and Oligomers of D-Amino Acid-Containing Peptides Using T-Wave Ion Mobility Mass Spectrometry. Journal of the American Society for Mass Spectrometry. 2017; 28(1):110–118. [PubMed: 27822705]
42. Lietz CB, Yu Q, Li LJ. Large-Scale Collision Cross-Section Profiling on a Traveling Wave Ion Mobility Mass Spectrometer. Journal of the American Society for Mass Spectrometry. 2014; 25(12):2009–2019. [PubMed: 24845359]
43. Han XL, Yang K, Gross RW. Multi-dimensional mass spectrometry-based shotgun lipidomics and novel strategies for lipidomic analyses. Mass Spectrometry Reviews. 2012; 31(1):134–178. [PubMed: 21755525]
44. May JC, Goodwin CR, Lareau NM, Leaptrot KL, Morris CB, Kurulugama RT, Mordehai A, Klein C, Barry W, Darland E, Overney G, Imatani K, Stafford GC, Fjeldsted JC, McLean JA. Conformational Ordering of Biomolecules in the Gas Phase: Nitrogen Collision Cross Sections Measured on a Prototype High Resolution Drift Tube Ion Mobility-Mass Spectrometer. Analytical Chemistry. 2014; 86(4):2107–2116. [PubMed: 24446877]
45. Dwivedi P, Schultz AJ, Hill HH. Metabolic profiling of human blood by high-resolution ion mobility mass spectrometry (IM-MS). International Journal of Mass Spectrometry. 2010; 298(1–3):78–90. [PubMed: 21113320]
46. Paglia G, Williams JP, Menikarachchi L, Thompson JW, Tyldesley-Worster R, Halldorsson S, Rolfsson O, Moseley A, Grant D, Langridge J, Palsson BO, Astarita G. Ion Mobility Derived Collision Cross Sections to Support Metabolomics Applications. Analytical Chemistry. 2014; 86(8):3985–3993. [PubMed: 24640936]
47. Winger BE, Lightwahl KJ, Rockwood AL, Smith RD. PROBING QUALITATIVE CONFORMATION DIFFERENCES OF MULTIPLY PROTONATED GAS-PHASE PROTEINS VIA H/D ISOTOPIC EXCHANGE WITH D2O. Journal of the American Chemical Society. 1992; 114(14):5897–5898.
48. Freitas MA, Hendrickson CL, Emmett MR, Marshall AG. Gas-phase bovine ubiquitin cation conformations resolved by gas-phase hydrogen/deuterium exchange rate and extent. International Journal of Mass Spectrometry. 1999; 185:565–575.
49. Suckau D, Shi Y, Beu SC, Senko MW, Quinn JP, Wampler FM, McLafferty FW. COEXISTING STABLE CONFORMATIONS OF GASEOUS PROTEIN IONS. Proceedings of the National Academy of Sciences of the United States of America. 1993; 90(3):790–793. [PubMed: 8381533]
50. Evans SE, Lueck N, Marzluff EM. Gas phase hydrogen/deuterium exchange of proteins in an ion trap mass spectrometer. International Journal of Mass Spectrometry. 2003; 222(1–3):175–187.
51. Chipuk JE, Brodbelt JS. Investigation of the gas-phase hydrogen/deuterium exchange behavior of aromatic dicarboxylic acids in a quadrupole ion trap. International Journal of Mass Spectrometry. 2007; 267(1–3):98–108.
52. Robinson JM, Greig MJ, Griffey RH, Mohan V, Laude DA. Hydrogen/deuterium exchange of nucleotides in the gas phase. Analytical Chemistry. 1998; 70(17):3566–3571. [PubMed: 9737208]
53. Freitas MA, Shi SDH, Hendrickson CL, Marshall AG. Gas-phase RNA and DNA ions. 1. H/D exchange of the M-H (−) anions of nucleoside 5′-monophosphates (GMP, dGMP, AMP, dAMP, CMP, dCMP, UMP, dTMP), ribose 5-monophosphate, and 2-deoxyribose 5-monophosphate with D2O and D2S. Journal of the American Chemical Society. 1998; 120(39):10187–10193.

54. Tian ZX, Lis L, Kass SR. Hydrogen-deuterium exchange and selective labeling of deprotonated amino acids and peptides in the gas phase. Journal of the American Chemical Society. 2008; 130(1):8–+. [PubMed: 18067298]
55. Pan JX, Heath BL, Jockusch RA, Konermann L. Structural Interrogation of Electrosprayed Peptide Ions by Gas-Phase H/D Exchange and Electron Capture Dissociation Mass Spectrometry. Analytical Chemistry. 2012; 84(1):373–378. [PubMed: 22129032]
56. Gucinski AC, Somogyi A, Chamot-Rooke J, Wysocki VH. Separation and Identification of Structural Isomers by Quadrupole Collision-Induced Dissociation-Hydrogen/Deuterium Exchange-Infrared Multiphoton Dissociation (QCID-HDX-IRMPD). Journal of the American Society for Mass Spectrometry. 2010; 21(8):1329–1338. [PubMed: 20452240]
57. Valentine SJ, Clemmer DE. H/D exchange levels of shape-resolved cytochrome c conformers in the gas phase. Journal of the American Chemical Society. 1997; 119(15):3558–3566.
58. Wyttenbach T, Bowers MT. Gas phase conformations of biological molecules: The hydrogen/deuterium exchange mechanism. Journal of the American Society for Mass Spectrometry. 1999; 10(1):9–14.
59. Rand KD, Pringle SD, Morris M, Brown JM. Site-Specific Analysis of Gas-Phase Hydrogen/Deuterium Exchange of Peptides and Proteins by Electron Transfer Dissociation. Analytical Chemistry. 2012; 84(4):1931–1940. [PubMed: 22235835]
60. Khakinejad M, Kondalaji SG, Maleki H, Arndt JR, Donohoe GC, Valentine SJ. Combining Ion Mobility Spectrometry with Hydrogen-Deuterium Exchange and Top-Down MS for Peptide Ion Structure Analysis. Journal of the American Society for Mass Spectrometry. 2014; 25(12):2103–2115. [PubMed: 25267084]
61. Maleki H, Maurer MM, Ronaghi N, Valentine SJ. Ion mobility, hydrogen/deuterium exchange, and isotope scrambling: Tools to aid compound identification in ‘omics mixtures. Analytical Chemistry. 2017; doi: 10.1021/acs.analchem.7b00075
62. Donohoe GC, Maleki H, Arndt JR, Khakinejad M, Yi J, McBride C, Nurkiewicz TR, Valentine SJ. A new ion mobility-linear ion trap instrument for complex mixture analysis. Analytical chemistry. 2014; 86(16):8121–8128. [PubMed: 25068446]
63. Tang K, Shvartsburg AA, Lee HN, Prior DC, Buschbach MA, Li FM, Tolmachev AV, Anderson GA, Smith RD. High-sensitivity ion mobility spectrometry/mass spectrometry using electrodynamic ion funnel interfaces. Analytical Chemistry. 2005; 77(10):3330–3339. [PubMed: 15889926]
64. Baker ES, Clowers BH, Li FM, Tang K, Tolmachev AV, Prior DC, Belov ME, Smith RD. Ion mobility spectrometry-mass spectrometry performance using electrodynamic ion funnels and elevated drift gas pressures. Journal of the American Society for Mass Spectrometry. 2007; 18(7):1176–1187. [PubMed: 17512752]
65. 1988.
66. Mesleh MF, Hunter JM, Shvartsburg AA, Schatz GC, Jarrold MF. Structural Information from Ion Mobility Measurements: Effects of the Long-Range Potential. J Phys Chem. 1996; 100(40):16082–16086.
67. Shvartsburg AA, Jarrold MF. An exact hard-spheres scattering model for the mobilities of polyatomic ions. Chemical Physics Letters. 1996; 261(1):86–91.
68. Khakinejad M, Kondalaji SG, Tafreshian A, Valentine SJ. Gas-Phase Hydrogen-Deuterium Exchange Labeling of Select Peptide Ion Conformer Types: a Per-Residue Kinetics Analysis. Journal of the American Society for Mass Spectrometry. 2015; 26(7):1115–1127. [PubMed: 25895891]
69. Campbell S, Rodgers MT, Marzluff EM, Beauchamp JL. Deuterium exchange reactions as a probe of biomolecule structure. Fundamental studies of cas phase H/D exchange reactions of protonated glycine oligomers with D2O, CD3OD, CD3CO2D, and ND3. Journal of the American Chemical Society. 1995; 117(51):12840–12854.
70. Solouki T, Fort RC, Alomary A, Fattahi A. Gas phase hydrogen deuterium exchange reactions of a model peptide: FT-ICR and computational analyses of metal induced conformational mutations. Journal of the American Society for Mass Spectrometry. 2001; 12(12):1272–1285. [PubMed: 11766754]

71. Paglia G, Angel P, Williams JP, Richardson K, Olivos HJ, Thompson JW, Menikarachchi L, Lai S, Walsh C, Moseley A, Plumb RS, Grant DF, Palsson BO, Langridge J, Geromanos S, Astarite G. Ion Mobility-Derived Collision Cross Section As an Additional Measure for Lipid Fingerprinting and Identification. Analytical Chemistry. 2015; 87(2):1137–1144. [PubMed: 25495617]

72. Tao L, McLean JR, McLean JA, Russell DH. A collision cross-section database of singly-charged peptide ions. Journal of the American Society for Mass Spectrometry. 2007; 18(7):1232–1238. [PubMed: 17512751]

73. May JC, Morris CB, McLean JA. Ion Mobility Collision Cross Section Compendium. Analytical Chemistry. 2017; 89(2):1032–1044. [PubMed: 28035808]

74. Valentine SJ, Counterman AE, Clemmer DE. A database of 660 peptide ion cross sections: Use of intrinsic size parameters for bona fide predictions of cross sections. Journal of the American Society for Mass Spectrometry. 1999; 10(11):1188–1211. [PubMed: 10536822]

75. Fenn LS, Kliman M, Mahsut A, Zhao SR, McLean JA. Characterizing ion mobility-mass spectrometry conformation space for the analysis of complex biological samples. Analytical and Bioanalytical Chemistry. 2009; 394(1):235–244. [PubMed: 19247641]

76. Valentine SJ, Counterman AE, Hoaglund-Hyzer CS, Clemmer DE. Intrinsic amino acid size parameters from a series of 113 lysine-terminated tryptic digest peptide ions. Journal of Physical Chemistry B. 1999; 103(8):1203–1207.

77. Shvartsburg AA, Siu KWM, Clemmer DE. Prediction of peptide ion mobilities via a priori calculations from intrinsic size parameters of amino acid residues. Journal of the American Society for Mass Spectrometry. 2001; 12(8):885–888. [PubMed: 11506220]

78. Ahmed A, Cho Y, Giles K, Riches E, Lee JW, Kim HI, Choi CH, Kim S. Elucidating Molecular Structures of Nonalkylated and Short-Chain Alkyl (n < 5, (CH2)(n)) Aromatic Compounds in Crude Oils by a Combination of Ion Mobility and Ultrahigh-Resolution Mass Spectrometries and Theoretical Collisional Cross-Section Calculations. ANALYTICAL CHEMISTRY. 2014; 86(7): 3300–3307. [PubMed: 24592806]

79. Hoadlund-Hyzer CS, Li JW, Clemmer DE. Mobility labeling for parallel CID of ion mixtures. Analytical Chemistry. 2000; 72(13):2737–2740. [PubMed: 10905301]

80. Li ZY, Dilger JM, Pejaver V, Smiley D, Arnold RJ, Mooney SD, Mukhopadhyay S, Radivojac P, Clemmer DE. Intrinsic size parameters for palmitoylated and carboxyamidomethylated peptides. International Journal of Mass Spectrometry. 2014; 368:6–14. [PubMed: 26023288]

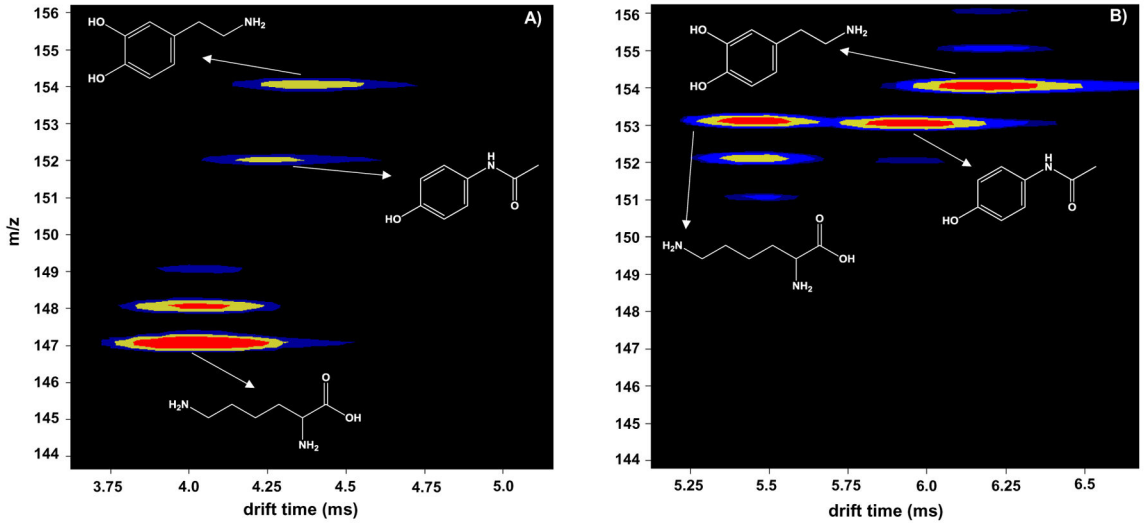

Figure 1.

Two-dimensional (2D) t_D, m/z plots for a mixture of lysine, acetaminophen, and dopamine A) in the absence of D_2O reagent gas and B) in the presence of D_2O reagent gas. Structures of ions associated to dataset features are indicated with arrows.

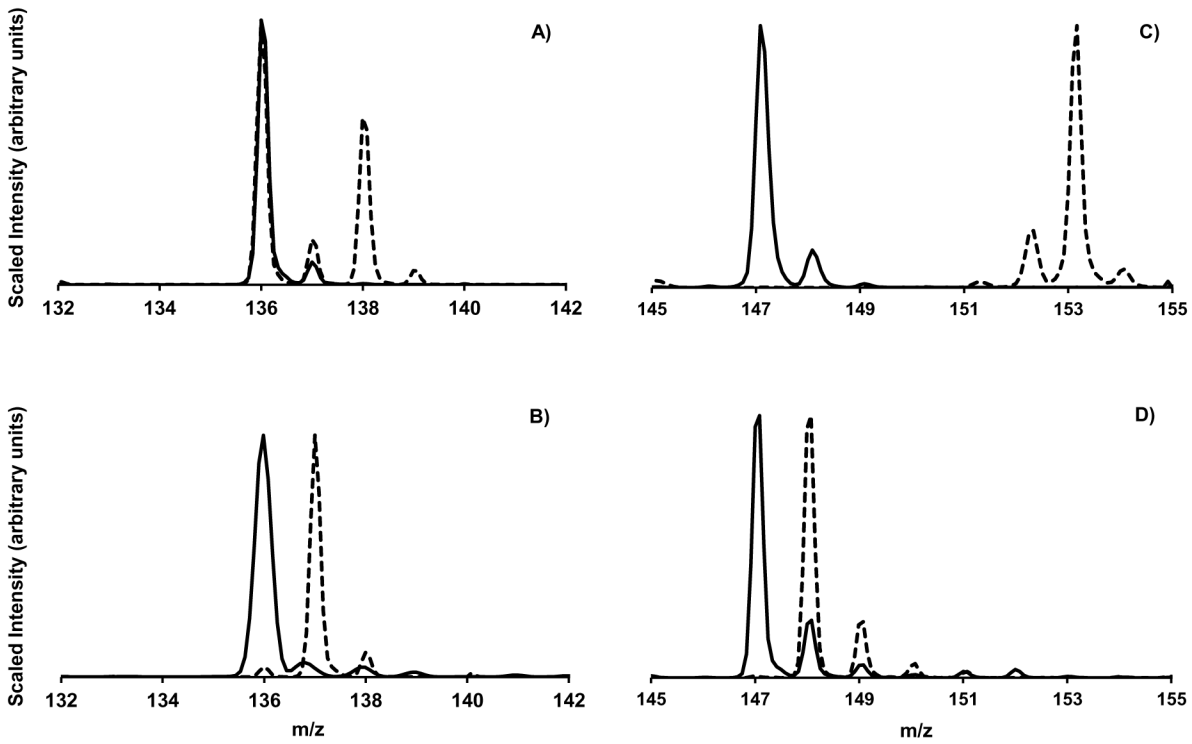

Figure 2.

Isotopic distributions for $[M+H]^+$ A) adenine and B) homocysteine ions and for $[M+H]^+$ C) lysine and D) glutamine ions. Solid lines show the distribution obtained in the absence of D_2O and the dashed lines show the isotopic distribution with the addition of ~0.04 Torr D_2O to the drift tube buffer gas.

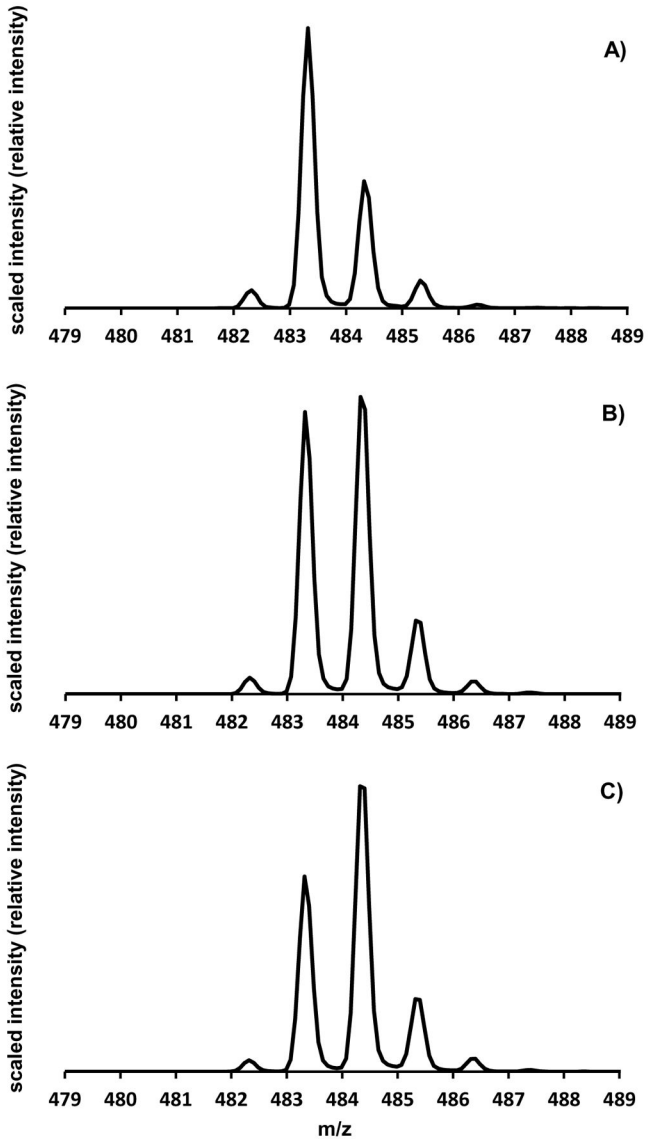

Figure 3.

Isotopic distributions for a mixture of two isobaric lipids (15:0 Lyso PC and 07:0 PC (DHPC)) at t_D selections of A) 10.8–11.0, B) 11.2–11.4, and C) 11.4–11.6 ms. The distributions were obtained using a D2O partial pressure of ~0.04 Torr.

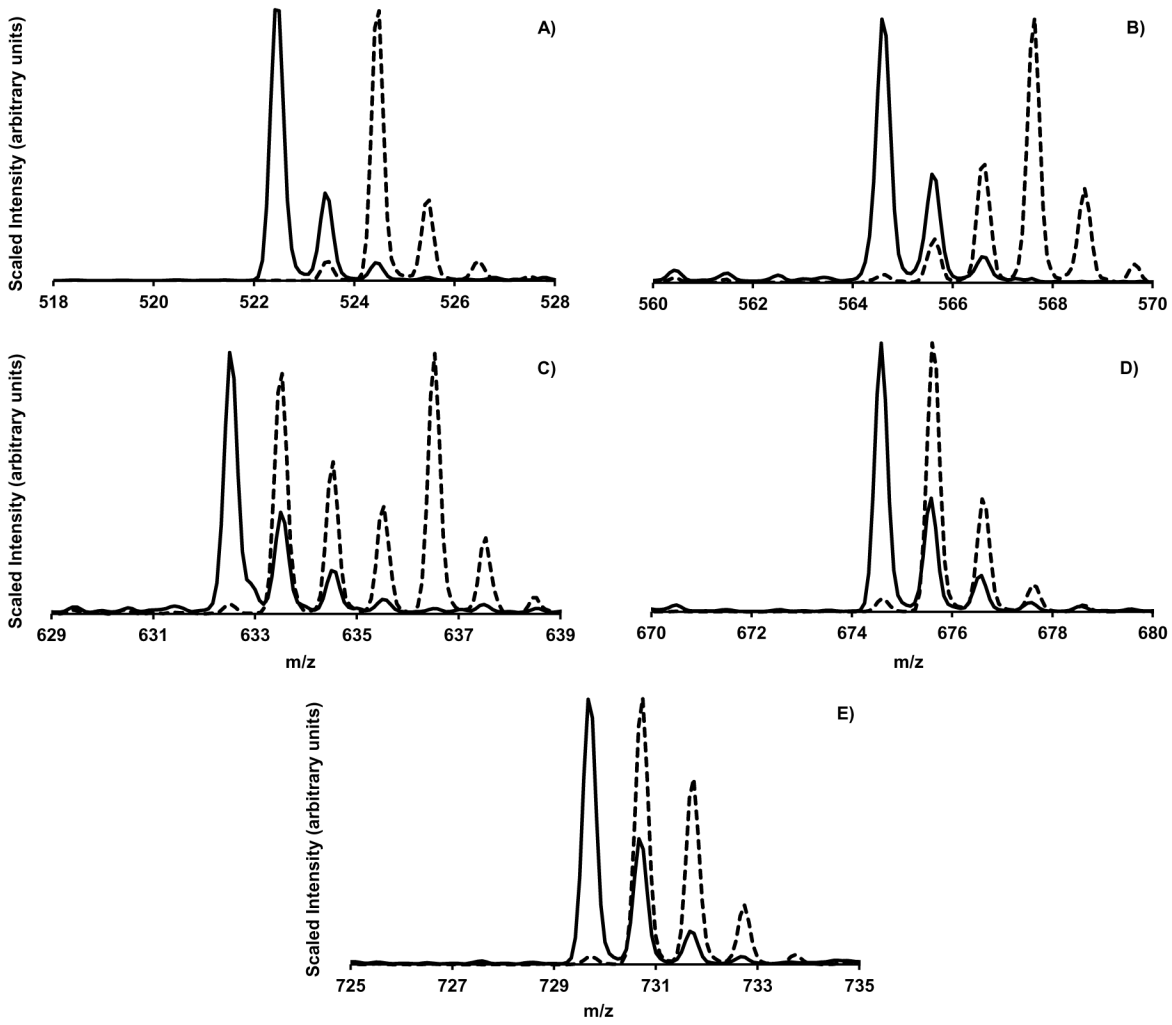

Figure 4.

Isotopic distributions for the A) M^+ 18:1 Lyso PC, B) $[M+H]^+$ 18:1 Ceramide, C) $[M+H]^+$ 14:1 PE, D) M^+ 14:1 PC, and E) M^+ 18:1 SM ions. Solid lines show the distribution obtained in the absence of D_2O and the dashed lines show the isotopic distribution with the addition of ~0.04 Torr D_2O to the drift tube buffer gas.

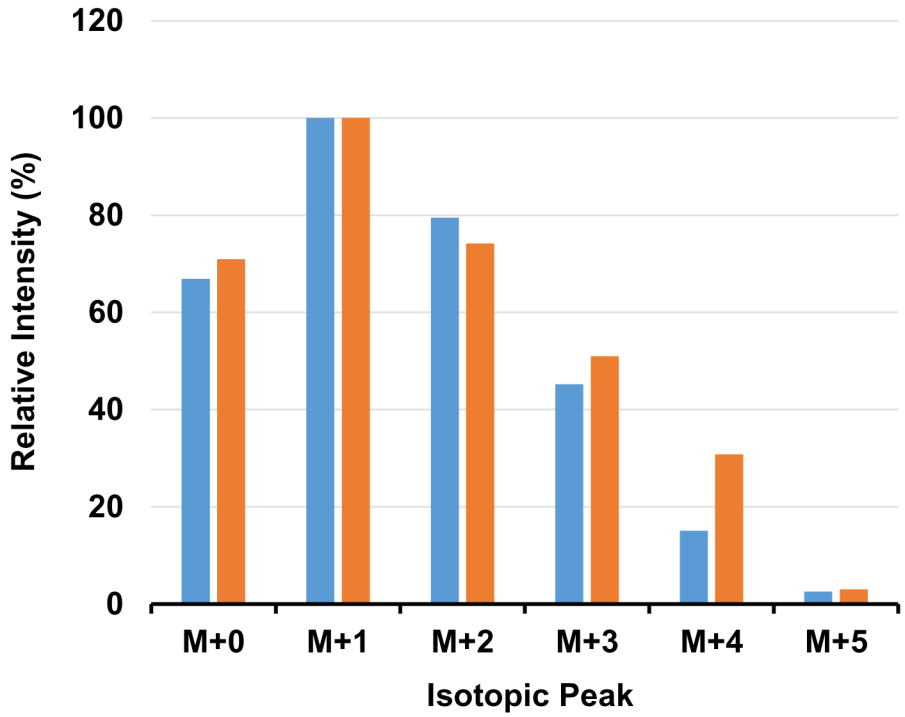

Figure 5.

Bar graph representing the isotopic distribution for $[M-H]^-$ sucrose ions upon addition of ~0.04 Torr D2O showing the relative intensities of the M+0, M+1, M+2, M+3, M+4, and M +5 peaks (red bars). The blue bars show the best-fit isotopic distribution obtained from the modeled isotopic distributions for in-silico candidate structures.

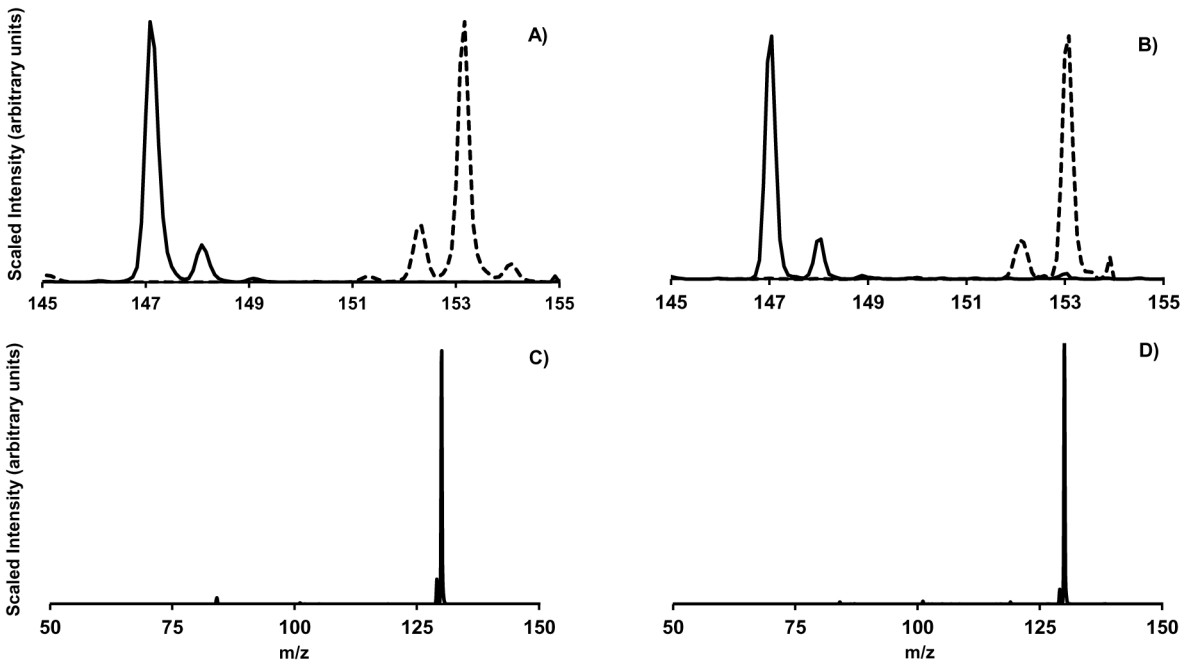

Figure 6.

Isotopic distributions obtained using a D_2O partial pressure of ~0.04 Torr for A) selected ions having a nominal *m/z* value of 147 from the bovine cardiac extract sample and B) $[M+H]^+$ lysine ions. Fragmentation patterns produced by CID of C) selected ions having a nominal *m/z* value of 147 from the bovine cardiac extract and D) $[M+H]^+$ lysine ions are also shown.

Table 1

Experimental $^{DT}CCS_{He}$ values calculated for the molecular standards.

Name	*m/z*[a]	Adduct[b]	Experimental $^{DT}CCS_{He}$[c]
Hydroxyproline	132.1	(M+H)	58.2
Leucine	132.2	(M+H)	64.3
Isoleucine	132.2	(M+H)	64.1
Adenine	136.1	(M+H)	57.4
Homocysteine	136.2	(M+H)	61.2
Glutamine	147.2	(M+H)	67.6
Lysine	147.2	(M+H)	64.7
Acetaminophen	152.2	(M+H)	69.2
Dopamine	154.2	(M+H)	70.8
Sucrose	341.3	(M-H)	112.4
15:0 Lyso PC	482.3	(M+H)	156.8
07:0 PC (DHPC)	482.3	(M+H)	155.4
18:1 Lyso PC	522.4	(M+H)	170.3
	544.4	(M+Na)	172.0
18:1 Ceramide	564.6	(M+H)	194.2
	586.6	(M+Na)	196.5
14:1 PE	632.5	(M+H)	185.4/193.0[d]
(Δ9-Cis) PC (14:1/14:1)	674.6	(M+H)	196.1
(Δ9-Trans) PC (14:1/14:1)	674.6	(M+H)	195.6
18:1 SM	729.7	(M+H)	220.9
	751.7	(M+Na)	222.4
18:1 TG	907.9	(M+Na)	269.7

[a] *m/z* recorded for each ion

[b] Adduct observed for each ion

[c] Experimental $^{DT}CCS_{He}$ values calculated from the measured t_D values

[d] $^{DT}CCS_{He}$ values reported for the two observed conformers belonging to ions of *m/z* 632.5 (Figure S3)